Prototype of Orthogonal Precoder-based Technique for Two-Tiered Cellular Networks

Leonardo S. Cardoso, Marco Maso, Ejder Bastug, Mérouane Debbah and Ozgur Ozdemir

***Abstract*— In [1], we introduced a spectrum sharing technique called Vandermonde-subspace frequency division multiplexing (VFDM). This overlay technique allows the coexistence of a downlink orthogonal frequency division multiplexing (OFDM) macro-cell and a cognitive small-cell in a time division duplex mode. In that work, VFDM was shown to be able to completely cancel the interference towards a primary macro-cell system at the price of perfect channel state information (CSI) at the opportunistic secondary small-cell. In this work, we propose the first prototype of VFDM transceiver as a first step towards a proof of concept of the complete technique. We focus on the secondary small-cell and, using the new SDR4All platform [2], we design the transmitter/receiver pair needed for our test. Logic and hardware details are provided, as well as user definable parameters. The obtained results are promising and show the practical feasibility of a VFDM transmission over secondary link.**

***Index Terms*—cognitive overlay network, interference cancellation, small-cells, VFDM**

I. INTRODUCTION

In a new trend of mobile communications, cellular networks are being enhanced with smaller base stations, known as small cells (SCs), as a means to improve capacity and coverage [3]. This new approach, uses cognition and awareness to effectively break off from the cellular structure constraints, increasing outdoor and indoor capacities. SCs (such as the LightRadios [4]) can be installed on top of lamp-posts, trees and other urban structures. A massively dense network of self-organizing and pervasive low powered radio nodes such as SCs could be the basis for a two-tiered network deployment, aiming at a more efficient spectrum usage. Nevertheless, this approach might generate unbearable amounts of cross-tier interference to legacy macro-cells, if unmanaged.

The tiered nature of the resulting network can be modeled from a cognitive radio perspective. In this scenario, the macro base stations and its user terminals act as the primary system, and SCs and its user terminals act as a secondary system. In such a framework, dynamic spectrum access (DSA) [5], can be adopted as a suitable strategy to manage the cross-tier interference. DSA can be implemented through various paradigms, i.e., overlay, underlay and interweave [6], differing in the adopted interference control mechanism [7], [8], [9].

In [1], we have proposed a novel technique for an overlay cognitive network deployment called Vandermonde-subspace frequency division multiplexing (VFDM). A secondary transmitter adopting VFDM can transmit over the same band as a primary transmitter, while canceling its interference to the latter, by means of a suitable linear precoder. This technique is based on a special Vandermonde matrix construction [10], and projects the signal to the secondary receiver on the null space of the interfering channel from the secondary transmitter to the primary receiver. VFDM benefits from the frequency selectivity of the channel to create a sort of frequency beamformer (similar to the classical spatial beamformer), and it can be applied to block transmission systems that exploit the redundancy provided by the introduction of a guard time, cyclic prefix or zero-padding.

In this contribution, we take a step further by introducing an implementation for the cognitive VFDM transmitter/receiver pair prototype. To the best of the author's knowledge, this is the first prototype proposal of VFDM transceiver. The work presented herein has been developed on the SDR4All platform [2]. This initial step serves as a proof of concept of the transmission part of VFDM and is essential to show an upcoming proof of concept of the full VFDM demonstrator.

This paper is organized as follows. In Sec. II, we introduce the considered cognitive channel model. We describe the SDR4All platform in Sec. III. In Sec. IV, we present the implementation guidelines for our prototype, transmitter/receiver side. In Sec. V, we show some experimental results obtained after a set of transmissions. Finally, conclusions and future research directions are discussed in Sec. VI.

In this work, we adopt the mathematical notation as described in the following. A lower case italic symbol (e.g. *b*) denotes a scalar value, a lower case bold symbol (e.g. **b**) denotes a vector, an upper case bold symbol (e.g. **B**) denotes a matrix. $[\mathbf{B}]_{m,n}$ denotes a matrix element at the m^{th} row and the n^{th} column. An $\boldsymbol{I}_{\mathrm{N}}$ denotes the identity matrix of size N. The transpose conjugate operator on a matrix is denoted by the H superscript (e.g.$\mathbf{B}^{\mathbf{H}}$), and the Moore-Penrose inverse matrix is denoted by † (e.g.$\mathbf{B}^{\dagger}$). All vectors are columns, unless otherwise stated.

II. SCENARIO

Consider two transmitter/receiver (TX/RX) pairs engaged in a downlink transmission. We assume that the secondary pair (TX2/RX2) wishes to communicate over the same band

L. S. Cardoso, M. Maso and M. Debbah are with Alcatel-Lucent Chair, Supélec, Gif-sur-Yvette, France (e-mail: {leonardo.cardoso, marco.maso, merouane.debbah}@supelec.fr). E. Bastug and O. Ozdemir are with Fatih University (e-mail: ejder.bastug@gmail.com, oozdemir@fatih.edu.tr)

This work is partially funded by CAPES-COFECUB, Fatih University scientific research fund under the project number P50061002 2 (1353) and Alcatel-Lucent, within the Alcatel-Lucent Chair in Flexible Radio, Supélec.

while avoiding harmful interference at the primary one (TX1/RX1). The two considered TX/RX pairs realize the so called cognitive interference channel (CIC), depicted in Fig. 1. According to the cognitive radio policy, the primary system, being the legal licensee of the band, is oblivious of the existence of the secondary system. Therefore, the former does not need to avoid interference to the latter.

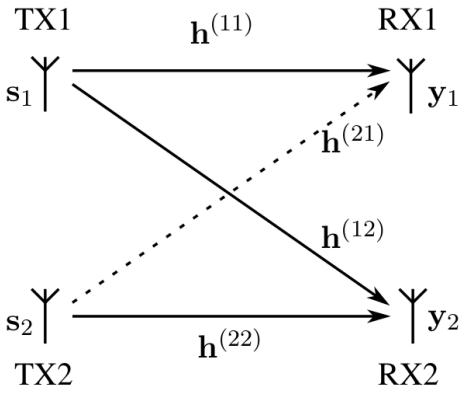

Figure 1 Cognitive interference channel model.

According to what is proposed in recent standards, i.e. LTE [11], we assume that TX1 adopts an $N+L$ block transmission system, i.e., an N subcarrier classical OFDM with cyclic prefix size of L. The redundancy introduced in these kinds of schemes to combat multipath and frequency selectivity (i.e., cyclic prefix) is seen as unused resources to exploit. Therefore, a linear precoder that projects the transmitted signal onto the null-space of the interfering channel from the secondary transmitter to the primary receiver can be found as detailed in the following section.

III. VFDM

Assuming a perfect synchronization at the reception at both systems, the received signals at RX1 and RX2 are respectively

$$\mathbf{y}_1 = \boldsymbol{F}\left(\mathbf{T}\left(\mathbf{h}^{(11)}\right)\mathbf{x}_1 + \mathbf{T}\left(\mathbf{h}^{(21)}\right)\mathbf{x}_2 + \mathbf{n}_1\right) \quad (1)$$

$$\mathbf{y}_2 = \mathbf{F}\left(\mathbf{T}\left(\mathbf{h}^{(22)}\right)\mathbf{x}_2 + \mathbf{T}\left(\mathbf{h}^{(12)}\right)\mathbf{x}_1 + \mathbf{n}_2\right), \quad (2)$$

where $\mathbf{T}\left(\boldsymbol{h}^{(ij)}\right) \in \mathcal{C}^{N\,x\,(N+L)}$ is a Toeplitz matrix modeling the convolution of the coded transmit symbols $\mathbf{x}_i$ with the channel $\left(\mathbf{h}^{(ij)}\right)$ [1], and $\boldsymbol{n}_i$ is an N-sized thermal noise vector. Note that, after a synchronization stage, RX2 discards the leading L received symbols to avoid inter-block interference (IBI), then performs a discrete Fourier transform (DFT). Thanks to this approach, conceptually, the only distinction between RX1 and RX2, is the connection to the respective transmitter. The modulated symbols vector transmitted by TX1 is

$$\mathbf{x}_1 = \mathbf{A}\mathbf{F}^{-1}\mathbf{s}_1 \quad (3)$$

where $\mathbf{A}$ is an $(N+L) \times N$ cyclic prefix insertion matrix, $\mathbf{F} \in \mathfrak{C}^{(NxN)}$ is a unitary DFT matrix with $[\boldsymbol{F}]_{k+1,l+1} = \frac{1}{\sqrt{N}} e^{-i2\pi\frac{kl}{N}}$, $k,l = 0,\dots,N-1$, and $\mathbf{s}_1$ is the N-sized uncoded transmit symbol vector.

Similarly to TX1, TX2 performs a $N+L$ block transmission, and its coded transmit symbol can be written as

$$\mathbf{x}_2 = \mathbf{E}\mathbf{s}_2\,, \quad (4)$$

Where $\mathbf{E}$ is a linear precoder and $\mathbf{s}_2$ is the uncoded transmit symbol vector, whose dimension will be detailed afterwards. By hypothesis, TX2 processes its signal such that, after the cyclic prefix removal at the RX1, the secondary interference signal is zero, that is

$$\mathbf{T}\left(\mathbf{h}^{(21)}\right)\mathbf{x}_2 = \mathbf{0}\,. \quad (5)$$

In [1] we show that, (5) holds true when perfect channel state information at the secondary transmitter (CSIT) is available, and we design $\mathbf{E}$ as an $(N+L) \times L$ Vandermonde matrix

$$\mathbf{E} = \begin{bmatrix} 1 & \cdots & 1 \\ a_1 & \cdots & a_L \\ a_1^2 & \cdots & a_L^2 \\ \vdots & \ddots & \vdots \\ a_1^{N+L-1} & \cdots & a_L^{N+L-1} \end{bmatrix}, \quad (6)$$

where $\{a_1, a_2, \dots, a_L\}$ are roots of the polynomial representation of the channel

$$\mathbf{h}^{(21)} = \textstyle\sum_{i=0}^{L} h_i z^{L-i}\,. \quad (7)$$

We note that the random distribution of the roots could lead to an ill conditioned precoder. Several methods can be adopted to solve this problem [1, 12]. In particular, we perform a Gram-Schmidt orthonormalization of the original Vandermonde matrix. At this stage, it is easy to see that due to the structure of the precoder $\mathbf{E}$, $\mathbf{s}_2$ has size L.

By construction, (5) is not dependent on either the realization or distribution of $\mathbf{s}_2$, thus VFDM ensures the effective interference cancellation irrespective of the primary and secondary system's transmitted data or power allocation. This is in contrast with what is proposed by techniques, which limit the maximum power used by the secondary system [13], hence limiting its usefulness only to short range communications [14].

IV. SDR4ALL

In this work, VFDM was implemented using a software/hardware platform called SDR4All. SDR4All is composed of a USB plug and play hardware part (i.e., USRPs), and a software part. It aims to bridge the gap between theory and practice, to reduce the time-to-market of ideas in telecommunications. Therefore, it has been developed for teaching and development in telecommunications and software radio. The hardware part is in charge of the RF and sampling processing while the radio transceiver's physical layer (PHY) is software driven, running in a computer.

All the baseband radio implementation takes place in a simplified environment, which is user friendly to theoretical engineers. Standard isotropic antennas made for the 2.4 and 5 GHz ISM band are adopted. The main parameters for the USRPs are provided in table I. As previously stated, the baseband is implemented in software, part of a MATLAB® toolbox developed specifically to this end. In order for the toolbox to correctly communicate with the USRPs, a driver was built.

TABLE I
PARAMETERS FOR THE HARDWARE PART.

parameter	value
Operating band	ISM 2.4 ~ 2.49 GHz
Baseband filtering	20 MHz
Channels	1 to 13 (802.11)
Total TX power	Up to 50 mW
Data bandwidth	Up to 16 MHz

It is able to transmit a given vector of baseband I/Q symbols and to listen for a certain amount of time and provide a vector of the received baseband I/Q samples. The driver also allows to configure the bandwidth and the center frequency for both transmission and reception. The toolbox implements basic communication blocks, such as bit operations, modulation, packet formatting and so on. Full communication chains are also implemented.

V. VFDM IMPLEMENTATION

Our goal is to show that a VFDM transceiver can be implemented in practice. In [1] a secondary transmitter can transmit data to the secondary receiver, while cancelling the interference towards the primary receiver, as shown in Fig. 2.

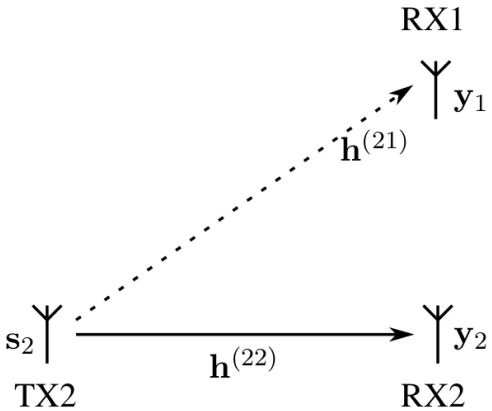

Figure 2 Cognitive secondary link.

Here we focus on the secondary link, the data transmission from TX2 to RX2. The experimental setup used to prove the feasibility of the VFDM based transmission is depicted in Fig. 3. As stated before, baseband signal processing is performed using the SDR4All toolbox, which is running in the operating system's user space. Let us initially focus on the secondary transmitter. The kernel driver of the toolbox handles the data streams and communicates with the USRP over USB link.

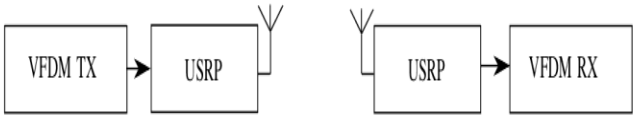

Figure 3 Experimental setup.

Inside the USRP, Cypress FX2 chipset receives the stream and sends it to Altera Cyclone FPGA for digital up-conversion from baseband to IF band. Inside the device, daughter-boards perform an analog up-conversion from IF to RF and finally the signals is transmitted over air through the antenna. More details about the hardware logic can be found in [19].

A. VFDM Baseband Transmitter

The block diagram of the VFDM transmitter is shown in Fig. 4. The input bit sequence to be transmitted is fed to the mapper. The mapped symbols are converted from serial to parallel according to the requirements of the VFDM precoder structure [1] (i.e., if the number of carriers used by the OFDM transmission in the primary system is *N*, with *L* cyclic prefix size, then the VFDM block precodes *L* parallel input symbols). We notice that, at this stage, the resulting stream can be modeled as a stream matrix **S**, of size *L* x *M*. Before the precoder stage, a pilot insertion block inserts pilot symbols for channel estimation purposes at the receiver (details on this operation are provided later).

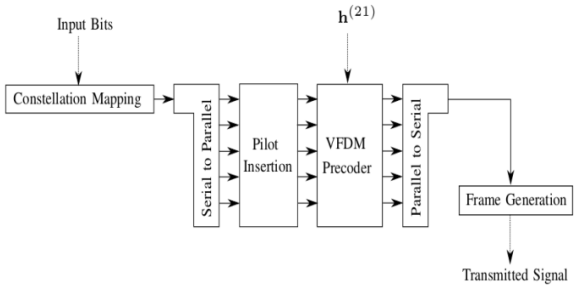

Figure 4 VFDM TX block diagram.

At this stage, a pilot symbol matrix **P** of size *L* x M_{PILOTS} is generated, such that

$$\begin{cases} [\mathbf{P}]_{k+1,l+1} = \alpha e^{-i2\pi \frac{kl}{M_{\mathrm{PILOTS}}}} \\ k = 0, \dots, L-1 \\ l = 0, \dots, M_{\mathrm{PILOTS}} - 1 \end{cases}, \quad (8)$$

Where M_{PILOTS} is a user defined parameter depending on the desired estimation accuracy. The pilot insertion is performed in two steps: 1) the input data stream is divided into $\frac{M}{N_{PILOTS}}$ groups of blocks composed by *L* symbols, where N_{PILOTS} is a parameter defining the number of repetition of **P** inside the considered frame, 2) a new stream is composed by alternating **P** to the groups of data blocks generated in the previous step as shown in Fig. 5. The sequence "pilots-data" is repeated until all the data to be transmitted is inside the payload.

The resulting stream is precoded inside the VFDM precoder block. In this work, we do not consider a specific channel estimation related to the link from the secondary

transmitter to the primary receiver. Therefore, the precoder is derived using an $L+1$ path Rayleigh fading channel realization $\mathbf{h}^{(21)}$, generated for test purposes and fed to the VFDM block to compute the Vandermonde matrix. A parallel to serial conversion adapts the precoded stream for the frame generation. In this phase, a preamble is added to the payload composed by data and pilot blocks. The resulting frame is depicted in Fig. 6.

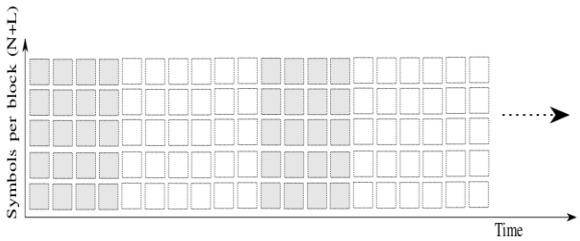

Figure 5 Output of the Pilot insertion block, the matrix P is denoted in gray.

The preamble is structured in two parts: 1) a Golay complementary sequence **g** [16] of length *N* taking values in {1+*j*, -1-*j*}, used at the receiver for time synchronization purposes, 2) a constant sequence of symbols **o** of size *bN* and value 1+*j*. This is introduced to assure correct detection of phase offset variations due to factors such as channel rotations, thermal noise at the receiver and imperfections in the phase lock loop (PLL), responsible for generating the carrier frequency at the chosen central frequency f_c.

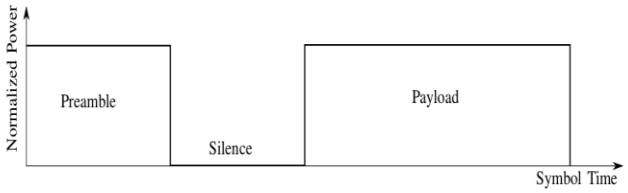

Figure 6 Frame Structure.

A constant sequence composed of zeros of size *cN*, acting as a guard time, is added between the preamble and the payload, for noise energy estimation at the receiver to compute signal-to-noise ratio. Note that *b* and *c* are natural numbers greater than 0.

B. VFDM Baseband Receiver

At the secondary receiver the hardware configuration is analogous and dual operations are performed (i.e., up-conversions become down-conversions and so on). The block diagram of the VFDM receiver is represented in Fig. 7. A critical and important aspect of VFDM is time synchronization. The interference cancelation can be effectively realized only through a precise cyclic prefix removal at RX1. We have to make sure that the signal transmitted by TX2 is synchronized with the primary transmission, otherwise the cyclic prefix removal procedure will discard the wrong part of the signal. In this case, RX1 would be prone to interference. Moreover, a time synchronization at symbol level has to be guaranteed, such that the payload can be correctly extracted from the received frame.

In this work, we focus on the secondary link, represented by the TX2/RX2 pair, hence we look at the synchronization problem from a symbol level perspective. The time synchronization of TX2 with RX1, is not an easy condition to guarantee, even in the simpler structured communication scenario (i.e., LTE). We will deal with this issue in a follow-up of this work, when the prototype of the full cognitive system will be presented.

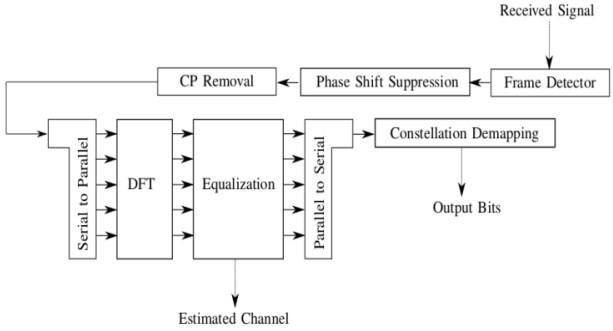

Figure 7 VFDM RX block diagram.

In the proposed implementation, RX2 exploits the payload structure, known beforehand. The purpose of this operation is to find the starting point of the VFDM frame with the highest possible accuracy. The autocorrelation of the Golay complementary sequence presents a clear peak for $m = 0$. This way RX2 can locate the first sample of the preamble, and synchronize with the input stream. By performing the cross-correlation between the received signal **y,** and the known Golay sequence **g**, that is

$$\mathrm{R}(n) \triangleq \sum_m \mathbf{y}^*(n)\boldsymbol{g}(n+m), \tag{9}$$

RX2 is able to detect $\hat{n}$, estimated starting point of the frame, by taking

$$\hat{n} = \max_n \mathrm{R}(n). \tag{10}$$

Once the time synchronization has been achieved, the receiver can estimate the phase shift of the received frame and suppress it. Similarly to what is proposed in recent standards [17, 18], in our scheme, RX2 compensates the phase shift of the whole frame through a two-step procedure. First, a *coarse* phase offset compensation is performed in order to mitigate the effect of the imperfections in the phase lock loop (PLL). We make use of the fact that, inside the preamble, **o** is composed of same-phase symbols. Therefore, the phase offset is estimated by

$$\widehat{\varphi_c} = \frac{1}{bN}\sum_{m=\hat{n}}^{\hat{n}+N(b+1)-1}(\varphi|r_{m+1}| - \varphi|r_m|). \tag{11}$$

where $\varphi|.|$ is the phase of a given complex value. Note that, each subsequent phase offset calculation is averaged out to compensate for phase noise. Once the *coarse* phase shift of the received VFDM frame is detected, a first compensation takes place. At this stage, we divide the preamble sequence in two equal portions, $\mathbf{o}_1$ and $\mathbf{o}_2$. The residual phase shift can be estimated and compensated adopting a similar approach to what is described in [17], then

$$\widehat{\varphi_f} = \frac{4}{(bN)^2}\sum_{m=\hat{n}}^{\hat{n}+\frac{N(b+1)}{2}-1} \varphi\left|r_m \, r^*_{m+\frac{N(b+1)}{2}}\right| . \qquad (12)$$

The authors are aware that other techniques better adapted to the same task exist, but this one was chosen due to its simplicity. The *fine* phase shift compensation ends the preamble processing, hence RX2 can start decoding the payload.

At this stage, RX2 starts decoding the frame. A cyclic prefix removal operation, followed by a serial to parallel conversion and DFT can be performed. The size of the packet at the output of the DFT block is equal to the number of carriers used in the OFDM primary system, that is *N*. The stream is then reorganized into a symbol matrix **T** of size N x $(M + M_{\text{PILOTS}}$ x $N_{\text{PILOTS}})$ and structure

$$\mathbf{T} = [\,\underline{\mathbf{D}}_1 \,|\, \underline{\mathbf{P}}_1 \,|\, \underline{\mathbf{D}}_2 \,|\, \underline{\mathbf{P}}_2 \,|\, \underline{\mathbf{D}}_3 \,|\, \dots\,], \qquad (13)$$

ready to be fed to the equalization block. In (11), $\underline{\mathbf{D}}_i$ is the i^{th} received data matrix of size N x $\frac{M}{N_{\text{PILOTS}}}$, and $\underline{\mathbf{P}}_i$ is the i^{th} repetition of **P** corrupted by the channel. Each occurrence of **P** inside the frame can yield a new equivalent channel estimation, used for subsequent equalization of the data symbols. RX2 does not have any information about the coherence time of the channel a priori. Therefore, by means of the repetition of the pilot symbol matrix **P**, the channel estimation can be updated frequently. This procedure can ensure that the system is able to cope with an in-frame channel rotation or change. Additionally, it may also correct a bad channel estimation due to an overly noisy environment. The i^{th} equivalent channel estimation is obtained by pilot evaluation as follows

$$\hat{\mathbf{H}}_i = \underline{\mathbf{P}}_i \mathbf{P}_i^{\mathbf{H}}, \qquad (14)$$

Being $\mathbf{P}_i\mathbf{P}_i^{\mathbf{H}} = \mathbf{I}_L$, by definition. Finally, the channel estimation can be used to equalize the received data, performing simple zero forcing equalizer [19]

$$\bar{\boldsymbol{D}}_i = \mathbf{H}_i^{+}\underline{\mathbf{D}}_i , \qquad (13)$$

where $\bar{\boldsymbol{D}}_i$ is the i^{th} equalized data matrix. After a parallel to serial conversion, the received symbols can be de-mapped into the output bit sequence.

We notice that the proposed VFDM receiver, re-uses the same decoding structure as a classic OFDM receiver, increasing the flexibility of the proposed solution. Nevertheless, we note that a peculiar characteristic of the VFDM architecture is represented by the pilot structure. In fact, the VFDM precoder accepts *L* symbols as an input, whereas the DFT block accepts *N*. This feature has a direct impact on the structure of the pilot symbol matrix that can be transmitted/received in the two systems.

VI. Experimental Results

To validate our model, and perform the VFDM transmission we set up a test bed composed of a TX/RX pair, managed by two laptops, as illustrated in Fig. 8. As described in Sec. III, the baseband signal processing is implemented at software level, exploiting a MATLAB® toolbox developed specifically to this end [20]. The SDR4All platform drives the hardware at both side of the transmission.

Figure 8 Transmission test bed

In the considered test, TX2 performs a set of 1000 transmissions, such that statistically relevant results can be obtained. The system configuration is described by the parameters in Table II.

TABLE II
USER DEFINED PARAMETERS.

Parameter	value
Carrier frequency	2.412 GHz
Bandwidth	4 MHz
N	128
L	16
N_{PILOTS}	$M/120$
M_{PILOTS}	10
Golay sequence length	128
Constant sequence length	2048
Zeros sequence length	128
Modulation Order	4-QAM

In this scenario, TX2 does not send any trigger message to the receiver before starting the communication, hence a repetition of the VFDM frame is transmitted, such that we make sure that RX2 can receive and buffer at least one frame. As we described in Sec V.A, TX2 inserts a guard band (i.e., zero sequence) between the preamble and the frame as shown in Fig. 6. This way, the receiver can estimate the experienced SNR during the preamble reception, by evaluating the received power during the second part of the preamble (i.e., the constant sequence), and the noise power during the silence. This measure serves as a first estimated of the SNR experienced at the receiver. The power profile of the received frame at RX2 is depicted in Fig. 9

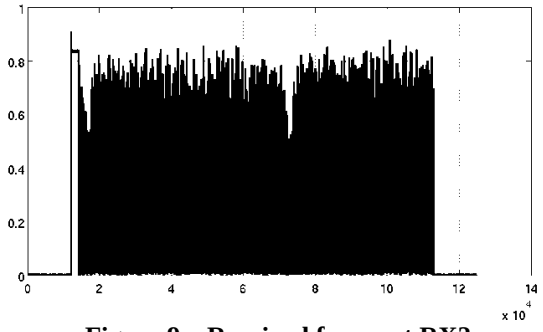

Figure 9 Received frame at RX2

In this case, the SNR experienced by the preamble is 25.8 dB. We note that the payload exhibits a very irregular power profile, especially if compared to the preamble. In particular, this points out a peak to average power ratio (PAPR) problem. Therefore, SNR for the payload can be different from the first estimation provided above. We investigate this problem by considering a sample of one of the aforementioned transmissions, depicted in Fig. 9, where (a) denotes the transmitted image and (b) the received one.

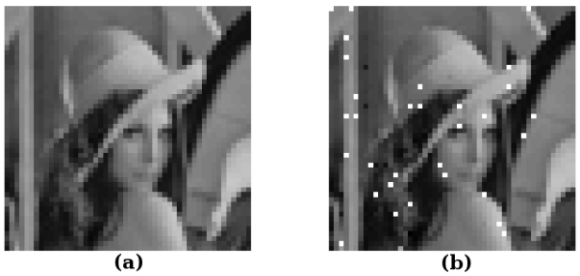

Figure 10 Transmitted and received image

First, we note that the proposed scheme for a standalone VFDM transmission is correctly working. On the other hand, looking at the picture, we observe that a transmission performed at high SNR is unlikely affected by the BER generating the faulty pixels in Fig. 9(b). Starting from this consideration, we characterize the BER behavior, and compute its cumulative distribution function (CDF), presented in Fig. 11.

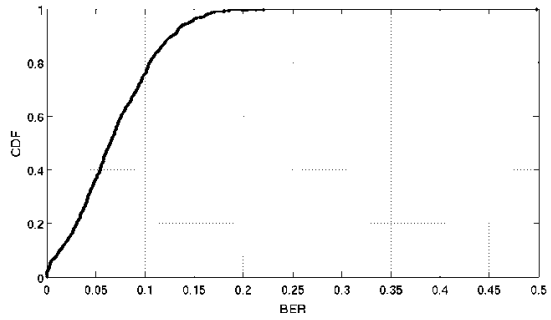

Figure 11 CDF of the BER

If we compare these results to what we obtained in [21], we can see that the average BER for SNR = 25 dB falls into the 10^{th} percentile of the obtained BER. Interestingly, the computed average BER has been 0.0703 that, according to [21], is the average BER of a transmission performed at SNR ~ 8 dB. These findings show that the preamble SNR and the BER of the transmission are not in a direct relationship, and that the experienced payload SNR has lower values. This is substantiated by Fig. 12, where the CDF of the preamble SNR is presented.

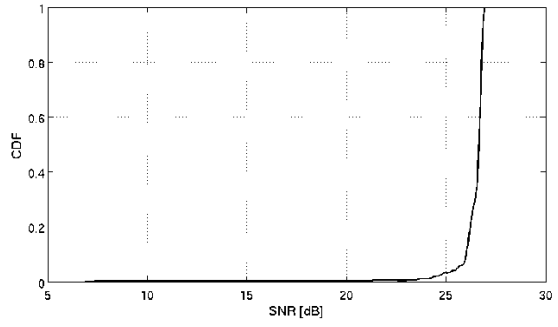

Figure 12 CDF of the preamble SNR

The CDF shows a very neat behavior, with an average value of SNR ~ 26 dB, confirming our previous results and enlightening the inadequacy of the preamble SNR to give a correct estimate of the payload SNR. Therefore, a rigorous understanding of the behavior of the power profile of the payload is required to fully characterize our system. To this goal, mechanisms to address the PAPR problem, and a more precise procedure to compute the payload SNR will be studied and implemented.

VII. CONCLUSION

This work shows how a VFDM transceiver can be designed and implemented and gives the first proof of concept of a working standalone VFDM transmission. The flexibility provided by the SDR4All platform allows for easy parameters tuning operation and configuration. The performed tests point out that we can not use the preamble SNR to have insights on payload SNR. Moreover, a PAPR problem in the payload has been shown. New procedures to characterize the power profile of the payload and address the current problems will be the subject of our future research. Nevertheless, the obtained results are encouraging and pose the basis for the future implementation of a complete cognitive VFDM based system.

REFERENCES

[1] L.S. Cardoso, M. Kobayashi, Ø. Ryan, and M. Debbah. "Vandermonde frequency division multiplexing for cognitive radio". In Proceedings of the 9th IEEE Workshop on Signal Processing Advances in Wireless Communications, pages 421–425, 2008

[2] [Online] http://www.flexible-radio.com/

[3] J. Hoydis, M. Kobayashi, and M. Debbah, "Green small-cell networks," Vehicular Technology Magazine, IEEE, vol. 6, no. 1, pp. 37-43, march 2011.

[4] Alcatel Lucent. "Lightradio: Evolve your wireless broadband network for the new generation of applications and users". [Online] Available: http://www.alcatel-lucent.com/features/light_radio/index.html, 2010.

[5] I. Akyildiz, W. Lee, M. Vuran, and S. Mohanty, "NeXt generation/dynamic spectrum access/cognitive radio wireless networks: a survey," Computer Networks, vol. 50, no. 13, pp. 2127-2159, 2006.

[6] A. Goldsmith, S. Jafar, I. Maric, and S. Srinivasa, "Breaking spectrum gridlock with cognitive radios: An information theoretic perspective," Proceedings of the IEEE, vol. 97, no. 5, pp. 894-914, 2009.

[7] W. Zhang and U. Mitra. "Spectrum shaping: A new perspective on cognitive radio (part I): Coexistence with coded legacy transmission". IEEE Transactions on Communications, 58(6):1857–1867, 2010.

[8] Y. Ma, D.I. Kim, and Z. Wu." Optimization of OFDMA-based cellular cognitive radio networks". IEEE Transactions on Communications, 58(8):2265–2276, 2010.

[9] S. Haykin. "Cognitive radio: brain-empowered wireless communications". IEEE Journal on Selected Areas in Communications, 23(2):201–220, 2005.

[10] G. Golub and C. Van Loan, Matrix Computations. Johns Hopkins University Press, 1996

[11] 3GPP TR 25.814, Physical Layer Aspects for Evolved UTRA, v.2.0.0. 3GPP, 2006.

[12] M. Kobayashi, M. Debbah, and S. Shamai, "Secured communication over frequency-selective fading channels: A practical Vandermonde precoding," 2009.

[13] A. Ghasemi and E.S. Sousa. "Fundamental limits of spectrum-sharing in fading environments". IEEE Transactions on Wireless Communications, 6(2):649–658, 2007.

[14] S.Srinivasa and S.A. Jafar. "The Throughput Potential of Cognitive Radio: A Theoretical Perspective". Fortieth Asilomar Conference on Signals, Systems and Computers, pages 221-225. 206

[15] F.A. Hamza. "The USRP under 1.5 X Magnifying Lens!". [Online] https://microembedded.googlecode.com/files/USRP_Documentation.pdf

[16] M.J.E. Golay. "Complementary series". IRE Trans. Inform. Theory IT-7: 82–87, 1961.

[17] Wireless LAN Medium Access Control (MAC) and Physical (PHY) Layer specifications – High speed physical layer in 5GHz band, [Online] http://standards.ieee.org/getieee802/download/802.11a-1999.pdf
[18] ETSI TS 101475 v1.2.2, Broadband Radio Access Networks (BRAN); HIPERLAN Type 2; Physical (PHY) layer, 2002
[19] D. Tse and P. Viswanath. Fundamentals of wireless communication. Cambridge University Press, 2005.
[20] [Online] http://www.flexible-radio.com/tools4sdr/
[21] Cardoso, L. S., F. R. P. Cavalcanti, M. Kobayashi, and M. Debbah, "Vandermonde-Subspace Frequency Division Multiplexing Receiver Analysis", PIMRC, Istanbul, Turkey, 2010.